Spatial Aerodynamic Roughness of Forested Landscapes from Airborne LiDAR

Mahmoud H. Ahmed[1], Roderik Lindenbergh[1], Massimo Menenti[1,2], Joris Timmermans[1]

[1] Department of Geoscience & Remote Sensing, Delft University of Technology, Delft, Netherlands
[2] State Key Laboratory of Remote Sensing and Digital Earth, Aerospace Information Research Institute, Chinese Academy of Sciences, Beijing, China

Keywords: Airborne Laser Scanning, AHN, Zero-Plane displacement, Aerodynamic roughness length, Eddy covariance, Landuse parameterization.

Abstract

Accurately representing forest canopies in atmospheric models remains challenging because trees interact with airflow in complex ways and strongly modulate surface–atmosphere exchanges. Aerodynamic roughness is therefore a key control variable in models of air quality, meteorology, and atmospheric transport. In this study, we test a physically based, spatially resolved framework for estimating aerodynamic roughness length from remote sensing observations. Using AHN (Actueel Hoogtebestand Nederland) airborne laser scanning data over a coniferous forest in Loobos, within the Veluwe Natura 2000 region in the central Netherlands, we derive geometric roughness parameters and compare them with eddy-covariance (EC) tower measurements. To further evaluate the approach, the LiDAR-derived roughness field is aggregated within sector-specific tower footprint climatologies and compared with tower-derived roughness estimates across 12 wind-direction sectors. Results show that LiDAR-based roughness captures strong directional and structural variability driven by forest stand height and canopy heterogeneity, closely aligning with the anisotropy observed in EC-derived displacement height and roughness length. The sector-wise comparison reproduces the main directional variability of tower-based aerodynamic roughness, although the LiDAR-derived values generally underestimate its magnitude, consistent with the distinction between structural and effective aerodynamic roughness. Seasonal differences between leaf-on and leaf-off conditions further highlight the role of canopy phenology in aerodynamic behaviour. The spatial patterns resolved by AHN demonstrate the potential of high-resolution laser scanning to capture fine-scale canopy–atmosphere interactions missed by traditional land-use-based roughness representations. This framework offers an observation-driven pathway for improving surface roughness parameterization in wind-flow and chemical transport models such as LOTOS–EUROS.

1. Introduction

Today, global environmental challenges are dominated by the dual forces of anthropogenic climate change and rapid human-driven changes in land-use (Clark et al., 2015). Together, these pressures underscore the need for refined dynamic modeling approaches that capture the full complexity of surface–atmosphere interactions (Steffen et al., 2005). Earth system models have progressed in recent years, from relatively static idealized representations of land–atmosphere exchanges to dynamic frameworks that integrate high-resolution observational data with process-level simulations (Van den Hurk et al., 2011). This evolution is expected to continue toward full digital twins of the environment (Bauer et al., 2021). Since the first attempts to incorporate land surface processes into climate models (Manabe et al., 1965; Manabe, 1969), land modeling has advanced to encompass detailed biogeophysical, biogeochemical and hydrologic processes (Sellers et al., 1997; Pitman, 2003). However, driving the simulations of these complicated processes requires large amounts of monitoring data to be integrated (de Koning et al., 2023). By assimilating essential information from satellites, ground-based sensor networks, and airborne platforms, modern environmental models can better represent transient surface properties. This can improve the characterization of energy and mass exchanges

Already several environmental digital twins are being developed, specifically focusing on climate change mitigation and extreme weather events. Likewise, environmental digital twins focused on biodiversity are presently being explored to deal with increasing pressure on natural ecosystems and habitats. By integrating chemical distribution models (such as LOTOS–EUROS (Manders et al., 2017)) with accurate ’real-time’ data, the spatio-temporal distribution of nitrogen can be estimated, and its impacts can then be investigated (Van Der Graaf et al., 2020). In these kinds of models, understanding how the Earth’s surface interacts with the lower atmosphere, at the land-atmosphere interface is crucial (Stull, 2012). In particular, aerodynamic roughness, as the key parameter in boundary layer meteorology, describes the resistance a surface imposes on airflow and governs how momentum is transferred between the atmosphere and the surface (Seginer, 1974; Weligepolage et al., 2012; Faivre et al., 2017). However, while this parameter in reality is dynamic and spatially variant, current models assume a single static value depending on land-cover (Dorman and Sellers, 1989; Wieringa, 1986). This reliance on static values overlooks local heterogeneity and seasonal changes. Furthermore, it often results in significant prediction errors when simulating surface energy budgets or flow over complex terrain (Floors et al., 2021).

Advances in remote sensing, especially LiDAR (Light Detection and Ranging) technology, now provide the potential to characterize the three dimensional canopy structure in detail (Boudreault et al., 2015). LiDAR enables the retrieval of profiles of essential structural metrics like frontal area index (λ_f) or plant area index (PAI). These variables can support dynamic roughness schemes that respond to local variations (Boudreault et al., 2015). These detailed, structure-based inputs can be used in wind modelling applications such as computational fluid dynamics (CFD) and in the estimation of parameters such as zero-plane displacement (d_0). Compared with traditional inputs,

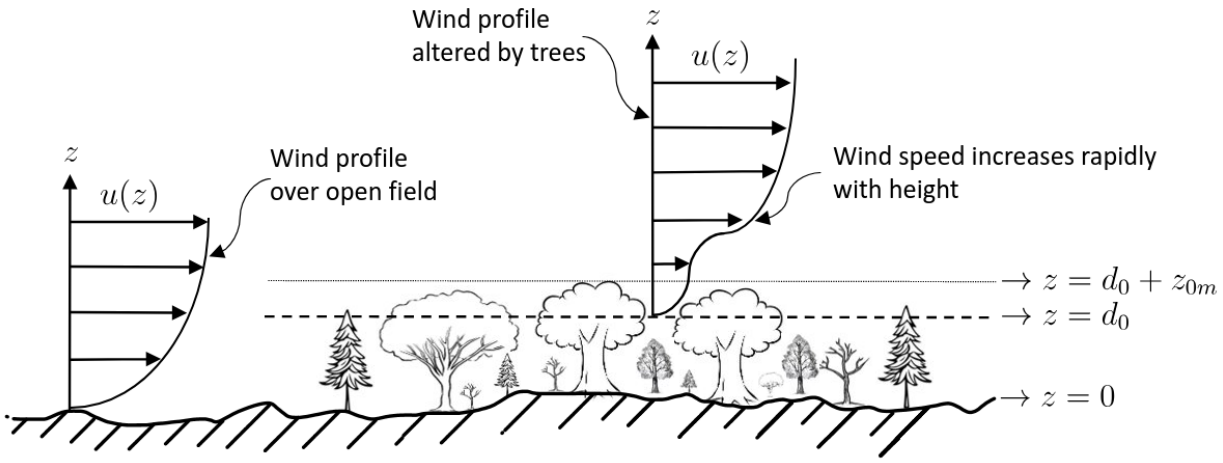

Figure 1. Conceptual illustration of the wind profile above open terrain and above a forest canopy. Over vegetated surfaces, the presence of trees modifies the vertical wind profile, shifting the effective origin of the logarithmic profile upward by the displacement height (d_0). The displacement height represents the level within the canopy at which the mean drag forces act and can therefore be interpreted as an effective ground surface for the flow. Below $z = d_0$, wind speeds are strongly attenuated and approach zero due to canopy drag. The roughness length for momentum (z_{0m}) defines the height above d_0 at which the extrapolated logarithmic wind profile becomes zero. The strong vertical gradient in wind speed above the canopy reflects the rapid acceleration of airflow as it adjusts from the highly resistive canopy layer to the freer atmosphere above.

they produce more accurate wind field predictions and reduce errors in wind resource assessment (Boudreault et al., 2015).

The objective of this study is to derive a physically based and spatially resolved representation of aerodynamic roughness length from AHN airborne laser scanning (ALS) data for the forested area of Loobos, within the Veluwe Natura 2000 region in the central Netherlands. The derived roughness estimates are validated against eddy covariance measurements from the ICOS[1] (Integrated Carbon Observation System) tower located at the site. By establishing a framework that links canopy structural attributes to aerodynamic properties, this work aims to improve the representation of turbulent fluxes and surface exchange processes in environmental models. The resulting parameterizations are intended to support refined land-use descriptions in wind flow and chemical transport modelling, thereby enhancing simulations of nitrogen transport and deposition across heterogeneous forest landscapes.

2. Background

2.1 Theory of Aerodynamic Roughness

Momentum exchange between the land surface and the atmosphere is commonly described using Monin–Obukhov Similarity Theory (MOST), where the roughness length for momentum (z_{0m}) and the zero-plane displacement height (d_0) (see Figure 1) represent the bulk effect of vegetation on the logarithmic wind profile (Monin and Obukhov, 1954; Shaw and Pereira, 1982). For neutral conditions, the mean wind speed (u) at a height z, follows

$$u(z) = \frac{u_*}{k} \ln\left(\frac{z - d_0}{z_{0m}}\right), \tag{1}$$

with u_* the friction velocity and k the von Kármán constant. Over forests, z_{0m} and d_0 are strongly governed by the geometry and height of the canopy, and the distribution of drag elements (Tian et al., 2011; Thom, 1971). Empirical parameterizations often relate both quantities to canopy height (e.g., $z_{0m} \approx 0.1h$, $d_0 \approx 0.6h$; where h is the canopy height) (Menenti and Ritchie, 1994). However, these simple relations overlook structural variability and are inadequate for heterogeneous canopies.

Traditional roughness parameterizations rely on coarse land-cover classes or visual inspection, which cannot resolve fine-scale spatial variation in forest structure (Kelly and Jørgensen, 2017; Floors et al., 2018). This motivates the use of physically based, geometry-driven, and data driven approaches that explicitly link canopy shape and density to aerodynamic behaviour.

2.2 Geometric Approaches and Existing Methods

Several frameworks exist to derive z_{0m} and d_0 from vegetation structure. The Objective Roughness Approach (ORA) uses fixed fractions of canopy height and is easy to apply but insensitive to canopy density or spatial heterogeneity (Thom, 1971; Enevoldsen, 2017). The Raupach formulation relates aerodynamic roughness to frontal area density and canopy drag properties, improving physical realism without the computational cost of turbulence-resolving models (Raupach, 1992, 1994). More complex schemes, such as SCADIS, incorporate detailed canopy profiles but require extensive parameterization and are less suited for operational mapping (Sogachev et al., 2002).

Geometric empirical models following Menenti and Ritchie (1994) provide an appealing compromise, as they derive aerodynamic parameters directly from the three-dimensional structure of the canopy. Moreover, they require only structural metrics that can be obtained from modern remote-sensing datasets. These approaches are particularly well suited to high-resolution LiDAR analysis, from which canopy height, drag-relevant geometry, and spatial variability can be retrieved with minimal assumptions.

[1] https://www.icos-cp.eu/about

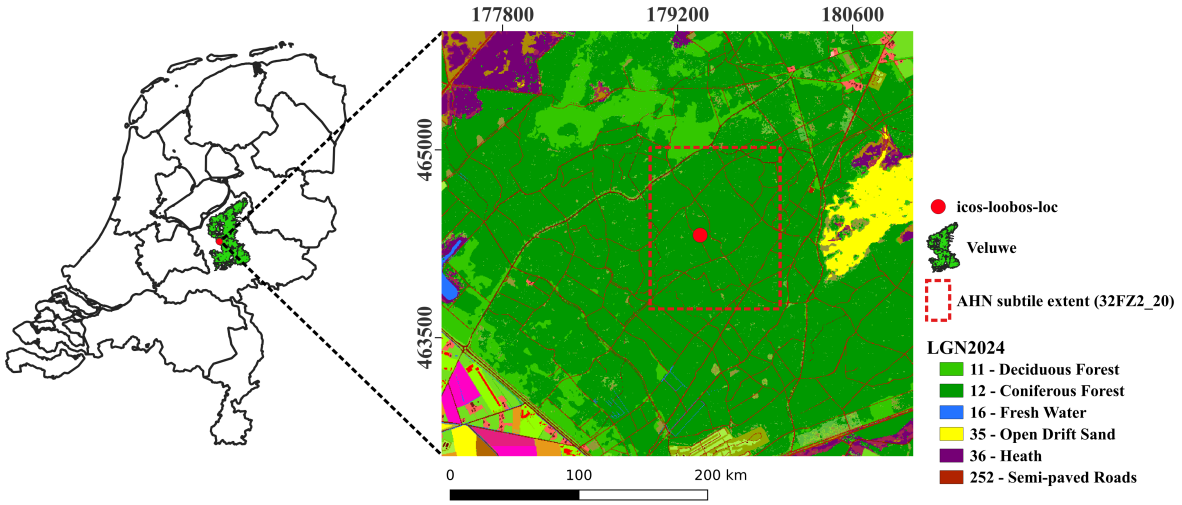

Figure 2. ICOS Loobos Tower location in the Veluwe area. The tower is indicated by a red dot. The LGN 2024 map shows the main land cover classes around the tower location and the legend highlights the most relevant ones.

2.3 LiDAR for Canopy Structure

Airborne laser scanning (ALS) enables detailed reconstruction of forest canopies, offering height, density, and geometric descriptors at metre-scale resolution (Beland et al., 2015; Bienert et al., 2010). Such structural metrics have been successfully linked to aerodynamic roughness in several studies (Queck et al., 2012; Floors et al., 2021), demonstrating that ALS provides the spatial detail needed to move beyond uniform or land-cover-based parameterizations. By quantifying the three-dimensional distribution of canoPackagepy elements, ALS allows roughness models to be driven by physical geometry rather than coarse empirical assumptions. In this study, we therefore adopt a geometric approach based on Menenti and Ritchie (1994), using ALS-derived structural metrics to estimate effective z_{0m} in a way that captures spatial variation across heterogeneous forest stands.

3. Materials & Methods

3.1 Study Area:

The study was conducted at the Loobos site (ICOS code NL-Loo[2]), located near Kootwijk in the Veluwe region, the Netherlands (52.166° N, 5.744° E; elevation ≈ 33 m a.s.l.) as depicted in figure 2. The site forms part of the Integrated Carbon Observation System (ICOS) network and hosts a Class 2 eddy covariance (EC) tower, which has been officially labeled since May 2023. The surrounding forest was established around 1909 on formerly active sand dunes, as part of a reforestation effort aimed at mitigating sand drift and providing timber for coal mining operations in the province of Limburg. Since its establishment, the forest has experienced minimal management intervention and now extends more than 1.5 km in all directions, forming a relatively homogeneous stand within the Veluwe landscape.

The dominant ecosystem type is an evergreen needleleaf forest, primarily composed of Scots pine (Pinus sylvestris) with an average canopy height of approximately 22 m. The region is characterized by a marine west coast (Cfb) climate, with a mean annual temperature of approximately 10.2 $^{\circ}C$ and an average annual precipitation of about 900 mm. The mean annual incoming shortwave radiation is 114 W/m^2. The area is part of the Ruisdael Observatory for Atmospheric Research [3], a national large-scale research infrastructure, supporting long-term observations and modeling of the atmospheric and terrestrial system.

3.2 AHN4 Airborne Laser Scanning Data:

The analysis relies on a high–resolution ALS tile from the fourth release of the Dutch national elevation dataset (AHN4). The selected subtile (`32FZ2_20`) was obtained via the TU Delft GeoTiles service (`https://geotiles.citg.tudelft.nl/`). The tile is provided in LAS 1.4 format (point format 8) and contains 69.78 million points. It covers an area of 1.34 km^2, and has a point density of 52.02 points m^{-2}.

The spatial extent of the tile is [175,980, 177,020] m in easting and [479,980, 481,270] m in northing. The dataset includes classified points for ground, water, and building returns, while all unclassified points (including vegetation) are stored in the ’others’ class. These data provide sufficient point density to resolve fine-scale canopy geometry relevant for aerodynamic roughness estimation.

3.2.1 Vertical Structure Analysis

Preprocessing and Height Normalization: ALS preprocessing consisted of basic quality control and height normalization. Outlier removal and point classification were handled using the provider-supplied attributes of the AHN dataset. Ground points were used to construct a local terrain model through inverse-distance–weighted interpolation, following the implementation in the `lidR` package (Roussel et al., 2020). Specifically, point heights were normalized using:

```
nlas <- lidR::normalize_height(las, lidR::knnidw())
```

[2] https://meta.icos-cp.eu/resources/stations/ES_NL-Loo

[3] https://ruisdael-observatory.nl/a-new-tower-in-loobos/

which applies a k-nearest neighbour inverse-distance weighting (KNN-IDW) ground interpolation. This procedure converts absolute elevations to heights above ground, ensuring that subsequent vertical analyses reflect true canopy structure independent of underlying terrain variability.

3.2.2 Geometric Estimation of Aerodynamic Roughness Length We estimate the effective aerodynamic roughness length ($z_{0,eff}$) directly from landscape geometry following the multi–scale approach of Menenti and Ritchie (1994). The method combines the structural contributions of low vegetation, sparse shrubs and trees, and terrain undulations into a single scale-aware expression:

$$z_{0,\mathrm{eff}} = \mathcal{F}\left(\underbrace{h_i, \sigma_{h,i}}_{\text{low vegetation}} , \underbrace{h, b, s, B, L}_{\text{shrubs/trees}}, \underbrace{a, \lambda}_{\text{topography}} \right), \quad (2)$$

where $(h_i, \sigma_{h,i})$ denote sub-window mean height (h_i) and height variability ($\sigma_{h,i}$). (h, b, s, B, L) describe obstacle geometry where h is the height of the shrubs/trees (meters), b is the base width of the vegetation (meter), B is the base width of the region with separated airflow (meters), s is the spacing of the vegetation (meter) ,and L is the restoration length of the logarithmic profile in the surface layer behind the obstacle. (a, λ) characterize the dominant topographic mode with a being the amplitude of relief described as periodic meters and λ is the wavelength of the relief in meters.

To derive the low vegetation roughness length $z_{0,\mathrm{veg}}$ from the AHN4 point cloud, we first selected vegetation points (`classification = 1`) and projected them onto a regular height grid with a resolution of 1 m. This grid defines the sub-pixel scale, at which local height variability is resolved. The estimation of $z_{0,\mathrm{veg}}$ is then performed at a coarser pixel scale of 5 m, corresponding to a moving window that aggregates 5×5 sub-pixel cells (Figure 3).

Within each pixel (estimation scale), the mean canopy height $\bar{h}$ is computed from all sub-pixel values. The pixel is further divided into N sub-pixel segments, and for each segment i, the local mean height h_i and standard deviation of height $\sigma_{h,i}$ are calculated. A constant noise floor $\sigma_0 = 0.05$ m is subtracted from $\sigma_{h,i}$ to account for residual measurement and processing noise, yielding the corrected variability $\max(\sigma_{h,i} - \sigma_0, 0)$.

The roughness length is then estimated as:

$$z_{0,\mathrm{veg}} = \frac{1}{N} \sum_{i=1}^{N} \left(\frac{\max(\sigma_{h,i} - \sigma_0,\, 0)}{h_i} \right) \bar{h}, \quad (3)$$

where $\bar{h}$ is the mean canopy height at the pixel scale, N is the number of sub-pixel segments within each pixel, and $\sigma_{h,i}$ and h_i represent the local variability and mean height within segment i, respectively.

To account for the mixture of herbaceous (low) vegetation and taller vegetation elements, the drag-partition formulation of Arya (1975) is commonly applied, as it redistributes momentum flux between the background surface and larger obstacles. The resulting mixed-scale roughness, $z_{0,\mathrm{mix}}$, depends on obstacle height, spacing, base width, and restoration length. However, because most of these parameters are difficult to retrieve in the dense forests of the Veluwe, where the understory is poorly resolved due to limited laser returns, this part of the analysis was not implemented. Instead, only the part that relates to obstacle height (h) was considered.

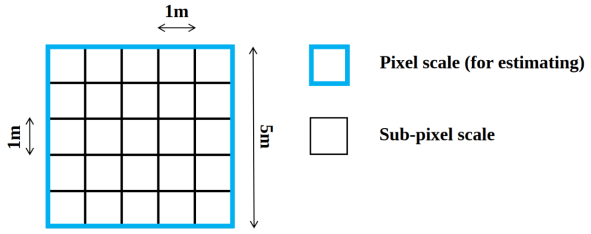

Figure 3. Illustration of the two-scale approach used to estimate $z_{0,\mathrm{veg}}$. The coarse pixel scale (5 m) defines the estimation window, while the finer sub-pixel scale (1 m) captures local height variability used in the roughness calculation.

To account for terrain-induced form drag, we applied the Taylor et al. (1987) correction to the LiDAR-derived tree roughness field on a window-by-window basis. For each roughness-estimation window, a matching patch was extracted from the AHN ground-surface DEM and detrended prior to spectral analysis. Specifically, the local topographic signal was isolated by removing the mean elevation, after which a two-dimensional Fast Fourier Transform (FFT) was applied to the detrended DEM patch. A Hanning window was used to reduce edge effects, and the resulting 2D periodogram was converted to a radially averaged 1D spectrum. To emphasize characteristic terrain scales rather than background spectral slope, the spectrum was normalized by a fitted power-law background. The dominant terrain wavelength, λ, was then identified from the peak of the normalized spectrum, while the corresponding topographic amplitude, a, was derived from the integrated spectral power within a narrow frequency band around that peak. These two quantities were subsequently used in the Taylor parameterization,

$$\ln\left(\frac{z_{0,\mathrm{eff}}}{z_{0,\mathrm{trees}}} \right) = 3.5 \left(a\, \frac{2\pi}{\lambda} \right)^2 \ln\left(\frac{\lambda}{z_{0,\mathrm{trees}}} \right), \quad (4)$$

to obtain the effective roughness length $z_{0,\mathrm{eff}}$ for each grid cell. Where the terrain patch was too small, too incomplete, or produced non-physical spectral estimates, no terrain correction was applied and the original $z_{0,\mathrm{trees}}$ value was retained.

To qualitatively evaluate the spatial consistency of the method, the resulting 5×5 m roughness estimation was compared against the corresponding rasterised AHN canopy height map, ensuring that the geometric formulation responds realistically to canopy structure and local terrain variability.

3.3 ICOS Loobos Eddy-Covariance Tower:

The Loobos tower hosts a complete eddy-covariance system providing 30-minute turbulent fluxes of momentum, sensible heat, as well as derived variables such as friction velocity (u_*), the Monin–Obukhov length (L), and the stability parameter ($\zeta = z/L$). All the fluxes measurements and parameters are recorded at a height of 38.2 m (Van der Molen et al., 2025a).

Complementary meteorological sensors record wind speed, wind direction, air temperature, humidity, and pressure at five vertical levels (2.4 m, 7.4 m, 15.7 m, 22.1 m, and 38.2 m) (Van der Molen et al., 2025b). For the present analysis, wind-speed measurements at 22.1 m ($WS\_2\_2\_1$) and 38.2 m

($WS\_2\_1\_1$) were used in combination with u_*, L, and ζ to estimate the displacement height (d) and surface roughness length (z_0). Quality-control procedures included removing flagged or missing observations (values = -9999), excluding low-turbulence periods ($u_* < 0.05$ m s^{-1}), and filtering out extreme stability conditions ($|z/L| > 5$). Furthermore, to minimize the stability effects, only data under neutral conditions ($i.e. -0.01 < \zeta < 0.01$) were considered.

The mean horizontal wind speed U_{mean} for each time step was computed as:

```
U_mean = ["WS_2_1_1", "WS_2_2_1"].mean()
```

and aggregated by wind-direction sector to provide the reference mean speeds used in the polar visualization of z_0 and d_0. These measurements offer an independent dataset for assessing directional variability in the LiDAR-derived roughness parameters.

3.3.1 Derivation of d and z_0 from EC Measurements The aerodynamic parameters were derived within the framework of MOST, assuming stationary and horizontally homogeneous flow in the surface layer. Following the logarithmic wind-profile formulation, the difference in mean wind speed between two levels z_1 and z_2 can be expressed as

$$\bar{u}(z_2) - \bar{u}(z_1) = \frac{u_*}{\kappa}\left[\ln\left(\frac{z_2 - d}{z_1 - d}\right) - \psi_m(\zeta_2) + \psi_m(\zeta_1)\right], \tag{5}$$

where $\kappa = 0.4$ is the von Kármán constant, $\zeta = (z - d)/L$ is the stability parameter, and $\psi_m(\zeta)$ is the integrated stability correction function. For unstable conditions ($\zeta < 0$), the Paulson–Businger formulation (Paulson, 1970), was applied, while for stable conditions ($\zeta > 0$) the empirical expression of Van Ulden and Holtslag (1985) was used.

Given measured values of u_*, $\bar{u}(z_1)$, $\bar{u}(z_2)$, and L, the displacement height d was determined iteratively using the above relation. The roughness length z_0 was subsequently obtained from the logarithmic wind equation evaluated at the upper level:

$$z_0 = (z_2 - d)\,\exp\left[-\frac{\kappa\,\bar{u}(z_2)}{u_*} - \psi_m(\zeta_2)\right]. \tag{6}$$

This two-level inversion approach yields site-specific estimates of d and z_0 directly from EC-derived turbulence parameters and wind-profile measurements, enabling their variation across wind directions and atmospheric stability regimes to be quantified for the Loobos forest canopy.

To ensure seasonal comparability with the AHN4 airborne laser scanning campaign (winter 2022), the analysis makes use of the earliest available ICOS Loobos flux data, starting in 2023. Two representative periods are selected: a leaf-off window from 2024-01-01 to 2024-03-31 and a leaf-on window from 2023-06-01 to 2023-08-31. These windows provide the closest seasonal match to the structural state of the forest at the time of the AHN4 acquisition and enable a consistent assessment of aerodynamic parameters under contrasting canopy conditions.

For a quantitative comparison between the tower-derived roughness estimates and the spatial $z_{0,\mathrm{eff}}$ field derived from AHN point clouds, it is necessary to account for the source area contributing to the tower measurements. This was done by computing the flux footprint at the wind-speed measurement height (38.2 m) using the Flux Footprint Prediction (FFP) method of Kljun et al. (2015).

4. Results

4.1 Spatial Patterns of Aerodynamic Roughness Length

Figure 4 presents the aerodynamic roughness length (z_0) estimated using the Menenti and Ritchie (1994) approach, alongside the rasterised AHN vegetation height and the corresponding LGN2023 land-use map. The z_0 field exhibits substantial spatial variability, reflecting the heterogeneous forest structure characteristic of the Veluwe. Higher values are concentrated in areas with tall, highly structured conifer stands, whereas lower values dominate in regions of shorter or more uniform vegetation. This behaviour is consistent with the sensitivity of the Menenti formulation to local height variability, which increases with crown complexity and multilayered canopies.

Although the roughness field is shown here at a 5 m resolution, this spatial scale is not intended for direct comparison with the tower footprint or for deriving footprint-representative aerodynamic parameters. Instead, the 5 m grid serves primarily as a qualitative diagnostic to assess the behaviour of the geometric method when applied to high–resolution ALS data. At this resolution, the map provides a clear visual check on the relationship between canopy structure and roughness magnitude, enabling us to verify that the formulation responds consistently to the fine-scale spatial heterogeneity present in AHN.

A notable feature is the presence of small gaps in the z_0 map. These discontinuities are not artefacts of the roughness estimation itself but arise from the input dataset. the (Menenti and Ritchie, 1994) algorithm was applied only to points classified as ”`Unclassified`”, which includes the vegetation in AHN, and the rasterised 5 m vegetation-height layer shows the same missing regions. These gaps correspond primarily to areas with insufficient point density or non-vegetated surfaces (e.g. roads, forest tracks, or very sparse cover), where the algorithm intentionally returns *NAN(Not A Number)* rather than an unreliable value.

Comparison with the AHN-derived canopy height (left panel) highlights the strong spatial coupling between vegetation structure and aerodynamic roughness. Regions with tall, spatially coherent canopy elements tend to produce elevated z_0 values, while height-homogeneous or low-growing vegetation results in markedly smaller roughness lengths.

Overall, the figure demonstrates that the geometric Menenti and Ritchie (1994) method captures the essential landscape-scale patterns in aerodynamic roughness, while preserving fine-scale spatial contrasts imposed by forest structure and land-use heterogeneity.

4.2 Seasonal Aerodynamic Roughness Derived from the ICOS Loobos Tower

Figure 5 presents the directional dependence of the displacement height (d) and aerodynamic roughness length (z_0) for

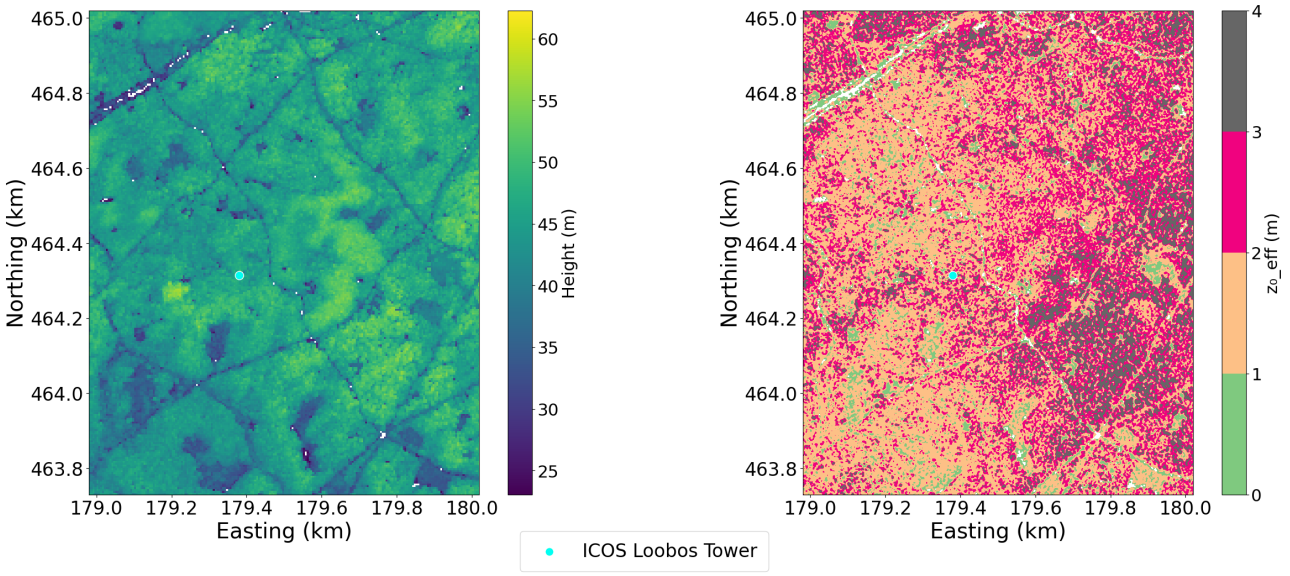

Figure 4. Spatial distribution of the aerodynamic roughness length z_0 (right) estimated using the geometric Menenti–Ritchie approach, compared with the rasterised AHN vegetation height (left). High roughness values coincide with tall, structurally complex coniferous stands, while lower values occur in short or homogeneous vegetation. The small gaps visible in the roughness map correspond to areas with insufficient AHN vegetation returns and are consistently observed in the 5 m rasterised AHN height layer, reflecting data limitations rather than methodological artifacts.

both the leaf-off (winter) and leaf-on (summer) periods, derived from paired wind-speed measurements at 22.1 m and 38.1 m at the ICOS Loobos tower. The leaf-on panels (Figure 5(c)–(d)) reproduce the expected anisotropy in canopy structure: the highest displacement heights (14.5–18.5 m) are observed for westerly and north-westerly winds (240°–330°), where the upstream forest is tallest and densest, whereas reduced values occur for south-easterly fetches (110°–160°), consistent with a more open stand structure. The corresponding roughness lengths vary between approximately 1.1 and 1.6 m and exhibit a similar directional pattern, with enhanced surface drag for westerly sectors and lower drag for easterly sectors.

The inclusion of leaf-off (winter) conditions (Figure 5(a)–(b)) reveals that aerodynamic parameters in this evergreen Scots pine stand exhibit detectable but modest seasonal variability. Winter values of d are on average 0.7 m higher than in summer, while z_0 differs by roughly 0.05 m, where both increases are consistent with wintertime changes in canopy aerodynamics such as reduced needle water content, altered needle posture, and reduced understory contribution. Importantly, the directional patterns remain largely consistent across seasons, reflecting the persistent influence of the surrounding heterogeneous canopy structure. These results demonstrate that, even in an evergreen needleleaf forest, aerodynamic properties are not static throughout the year; instead, they respond to subtle seasonal changes in canopy morphology and atmospheric conditions, while preserving strong directional anisotropy imposed by the landscape structure around the tower.

4.3 Qualitative and Quantitative explanation of EC vs. LiDAR differences

The comparison between EC-derived aerodynamic parameters and those obtained from the LiDAR-based geometric method reveals systematic and scale-dependent differences. In a heterogeneous forest such as the Veluwe, the EC footprint integrates contributions from broad upwind areas, which often include both tall stands and more open or lower-roughness patches. This spatial averaging tends to moderate the effective displacement height and roughness length inferred from the momentum fluxes. In contrast, the LiDAR estimates are strictly local and therefore strongly influenced by the immediate canopy structure surrounding the tower.

This distinction is most evident in the roughness length, where the LiDAR-based values are typically a factor of $2-4$ higher than their EC-derived counterparts. The geometric Menenti–Ritchie formulation quantifies roughness directly from crown variability and height contrasts within each tile, making it highly sensitive to local structural complexity—especially sharp changes in canopy height, crown edges, and clustering. These features exert a strong geometric signature but do not necessarily translate into proportional drag at the scale of the EC footprint, where the momentum flux is shaped by a much larger and more heterogeneous landscape.

To move beyond this qualitative interpretation, a footprint-based quantitative comparison was performed. The EC flux footprint was computed using the Kljun et al. (2015) FFP model, both as a climatological footprint (aggregated over all wind directions) and at the level of individual directional sectors (30° bins). The resulting footprints were overlaid on the LiDAR-derived $z_{0,\mathrm{eff}}$ map (Figure 6), and roughness values within the 80% cumulative footprint were used to obtain spatially representative estimates.

The footprint climatology (Figure 6, left) shows that the majority of the flux contribution originates from a relatively compact upwind area, with the 80% contour extending approximately $1\ \mathrm{km}$ in the streamwise direction and about $0.5\ \mathrm{km}$ laterally. This source area remains fully contained within the AHN subtile, ensuring consistency between the EC observations and the LiDAR-derived roughness field. The footprint is slightly elongated in the prevailing wind direction, reflecting the dominant contribution of westerly flows at the site.

This contribution has been peer-reviewed. The double-blind peer-review was conducted on the basis of the full paper.
https://doi.org/10.5194/isprs-annals-XI-3-2026-695-2026 | © Author(s) 2026. CC BY 4.0 License.

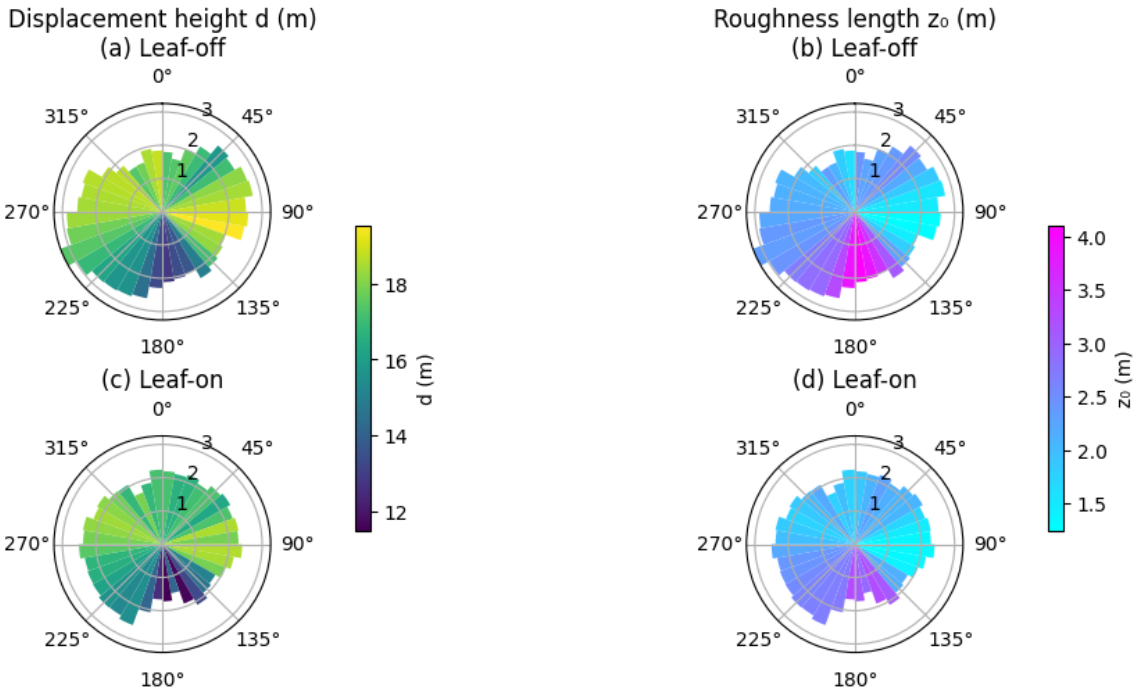

Figure 5. Directional dependence of the displacement height (d) and aerodynamic roughness length (z_0) at the ICOS Loobos forest site for leaf-on (summer) and leaf-off (winter) conditions. Panels (a) and (b) show the winter estimates of d and z_0, while panels (c) and (d) present the corresponding summer values. All panels use the same color scale per variable to facilitate seasonal comparison. Wind directions are grouped into 36 sectors (10° bins), and in each polar plot the radial extent of the bars represents the mean wind speed (in m s^{-1}; radial ticks at 1, 2, and 3), while the bar colour encodes the magnitude of d or z_0. Both variables exhibit pronounced azimuthal variability reflecting the heterogeneous stand structure surrounding the tower, with higher aerodynamic parameters for westerly and south-westerly winds and lower values for eastern sectors. Winter values show slightly elevated d and z_0 overall, consistent with seasonal changes in canopy aerodynamic behaviour, while maintaining the same directional patterns imposed by the surrounding forest.

At the sector level (Figure 6, right), the footprint becomes more directional and spatially confined, clearly illustrating how the source area shifts with wind direction. This sector-specific footprint was used to aggregate $z_{0,\mathrm{eff}}$ values for direct comparison with the corresponding EC-derived roughness estimates. The comparison confirms that accounting for the footprint reduces the scale mismatch between the two approaches, although systematic differences remain due to the intrinsic distinction between local structural roughness and effective aerodynamic roughness.

To allow a directionally consistent comparison between the tower-derived aerodynamic roughness length and the LiDAR-based roughness field, the filtered eddy-covariance observations were divided into 12 wind-direction sectors of 30° each. For each sector, the tower-based roughness length z_0 was aggregated from the corresponding subset of observations, while a sector-specific footprint climatology was computed with the FFP approach using the same subset of meteorological conditions. The LiDAR-derived roughness field $z_{0,\mathrm{eff}}(x, y)$ was then interpolated to the footprint grid and aggregated within the area enclosed by the 80% footprint contour using the footprint function as a spatial weighting kernel. This yielded, for each sector, a LiDAR-based effective roughness value directly comparable to the sectoral tower estimate.

The comparison showed a generally consistent directional pattern, but also a systematic negative bias of the LiDAR-based roughness relative to the tower-derived z_0. Across the 12 sectors, the median bias was -0.43 m, the median absolute relative error was 23%, and the median absolute $\log_{10}$ ratio was 0.106, corresponding to a typical multiplicative mismatch of about 1.28. The root-mean-square error (RMSE) was 0.90 m, increasing to 1.06 m when weighted by the number of samples per sector. These results suggest that the LiDAR-based roughness metric captures the main directional variability of the aerodynamic roughness, but tends to underestimate its magnitude, likely because the structural roughness representation does not fully account for all aerodynamic processes integrated by the tower measurements.

5. Discussion

The aerodynamic parameters derived from the ICOS Loobos tower reveal a clear directional dependence that reflects the heterogeneous forest structure surrounding the site. The azimuthal variability in both displacement height (d) and roughness length (z_0) is consistent with earlier work that showed that canopy architecture and stand heterogeneity impose strong directional signatures on momentum exchange (Shaw and Pereira, 1982; Finnigan, 2000). Importantly, even though the surrounding area is uniformly classified as coniferous forest on land-use maps, the tower data show that height and structural differences within this single class exert dominant control on its aerodynamic response. The highest values of d and z_0 occur in the taller, denser north–western and south–western sectors, while lower values correspond to shorter or more open patches. This demonstrates that the height of the forest stand, and not land-use class alone, dictates the roughness characteristics. Furthermore, even mod-

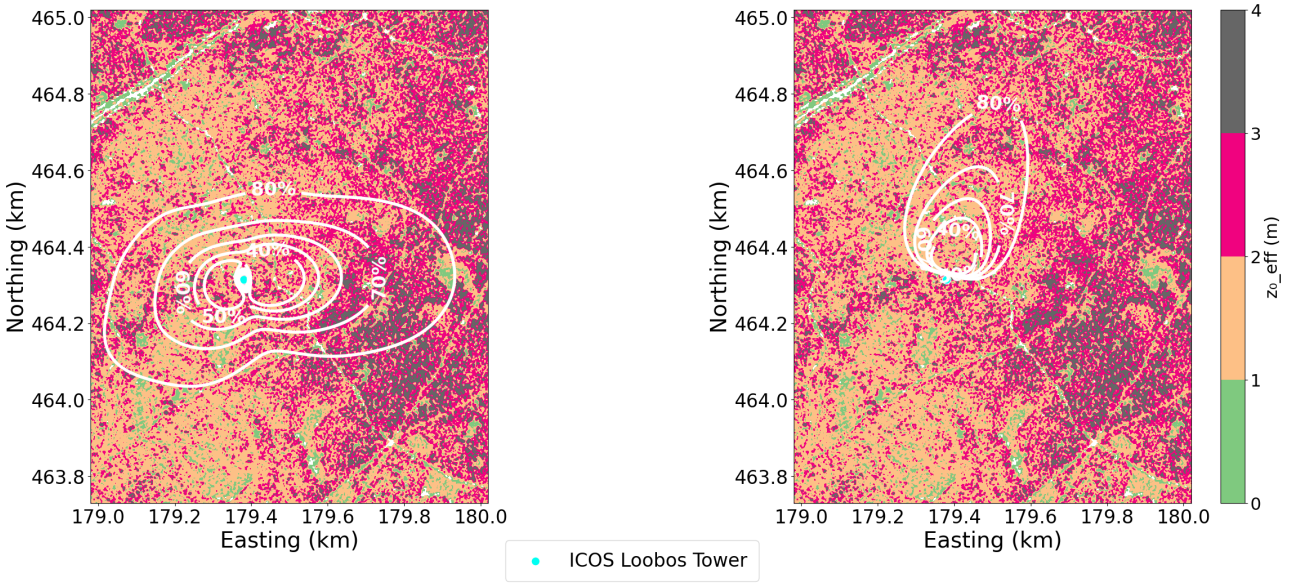

Figure 6. Flux footprint analysis overlaid on the LiDAR-derived effective roughness field ($z_{0,\mathrm{eff}}$). The left panel shows the footprint climatology during leaf-off conditions, aggregated over all wind directions, while the right panel presents the footprint for a representative 30° wind sector. White contours indicate cumulative source areas (40%, 50%, 60%, 70% and 80%). The 80% contour in the climatological footprint extends approximately 1 km in the main wind direction and about 0.5 km laterally, indicating that the dominant flux source area is well contained within the AHN subtile. The elongated footprint shape reflects prevailing wind directions and highlights the anisotropic nature of the source area. The sector-specific footprint (right) demonstrates how the contributing area becomes more focused and directionally dependent, enabling a consistent aggregation of $z_{0,\mathrm{eff}}$ for comparison with EC-derived aerodynamic parameters.

est structural variability within a nominally homogeneous class produces measurable aerodynamic anisotropy.

A notable outcome is the seasonal shift in aerodynamic characteristics between the winter (leaf-off) and summer (leaf-on) periods. This pattern suggests that the foliage changes the effective canopy roughness in summer by filling in the structural gaps between branches and trunks. In winter, these exposed elements interacts with higher wind speeds, that increases both displacement height and roughness length. This seasonal contrast aligns with previous observations that the leaf area modulates the vertical distribution of drag and alters the effective roughness interface (Finnigan, 2000), highlighting the critical role of phenology in realistic aerodynamic parameterization.

The LiDAR-derived roughness reproduced the main sectoral variability of the tower-based aerodynamic roughness, but generally underestimated its magnitude. This is consistent with the conceptual difference between the two quantities: the AHN-based metric represents canopy structure, whereas the eddy-covariance estimate reflects the effective aerodynamic response of the surface, including flow interaction and drag distribution, which are not driven by geometry alone, especially under heterogeneous forest conditions. These results therefore support the use of LiDAR-derived roughness as a structurally meaningful proxy, while also indicating that its evaluation should ideally be extended to the full footprint domain. In the present analysis, however, the full footprint often extended beyond the AHN subtile, reaching source areas on the order of $O(2\ \mathrm{km})$ from the tower. A logical next step is therefore to repeat the comparison using a full AHN tile in order to assess the LiDAR-based roughness over the complete source area seen by the tower. In addition, part of the systematic underestimation may have stemmed from the decision to omit part of the drag-partition correction associated with trees (in Arya (1975)), which would otherwise account for the additional roughness contribution of larger vegetation elements.

A broader implication of these findings is the clear limitation of static roughness representations currently used in atmospheric chemistry and deposition models such as LOTOS-EUROS (Manders et al., 2017). These models rely on land-use classes derived from products like CORINE (100 m resolution) combined with static lookup tables for roughness parameters. Our results show that such an approach fails to capture the substantial variability that exists within a single land-use class due to height differences, structural complexity, and phenological state. Consequently, the dynamic and directionally varying patterns observed in both the tower and point-cloud data are entirely missed by current operational roughness schemes. Incorporating structure-aware, LiDAR-informed roughness estimates into these models would therefore provide a more physically grounded and spatially realistic representation of canopy–atmosphere interactions.

6. Conclusion and Future Work

This study combined Eddy-Covariance estimates of aerodynamic roughness with LiDAR-derived structural roughness to investigate canopy–atmosphere interactions at the ICOS Loobos site. The results showed that stand height and structural heterogeneity produce clear directional variability in both displacement height and roughness length, even within a single forest type, and that seasonal differences further influence these aerodynamic properties. The LiDAR-derived roughness reproduced the main sectoral variability of the tower-based z_0, but generally underestimated its magnitude, reflecting the expected distinction between structural and aerodynamic roughness. Overall, the analysis highlights the added value of structure-

aware roughness estimates over static land-use-based parameterizations such as those commonly used in LOTOS-EUROS.

Future work should extend the comparison to a full AHN tile, since the full tower footprint frequently exceeded the spatial extent of the current AHN subtile. It will also be important to benchmark the present geometric approach against both the default roughness parameterization used in LOTOS-EUROS and more physically based models such as Raupach (1994). Finally, validation should be expanded beyond Loobos by comparing against EC observations from another tower in a contrasting forest structure or in terrain with more pronounced relief, in order to test the robustness and transferability of the method.

Data availability

All scripts and functions used for the numerical calculations and figure generation presented in this manuscript are available on GitHub at `https://github.com/Mahmoud-H97/effective_roughness`.

References

Arya, S., 1975. A drag partition theory for determining the large-scale roughness parameter and wind stress on the Arctic pack ice. *Journal of Geophysical Research*, 80(24), 3447–3454.

Bauer, P., Stevens, B., Hazeleger, W., 2021. A digital twin of Earth for the green transition. *Nature Climate Change*, 11(2), 80–83.

Beland, M., Parker, G., Harding, D., Hopkinson, C., Chasmer, L., Antonarakis, A., 2015. White paper—On the use of LiDAR data at AmeriFlux sites. *Ameriflux Network, Berkeley Lab: Berkeley, CA, USA*.

Bienert, A., Queck, R., Schmidt, A., Bernhofer, C., Maas, H., 2010. Voxel space analysis of terrestrial laser scans in forests for wind field modelling. *International archives of photogrammetry, remote sensing and spatial information sciences*, 38(Part 5), 92–97.

Boudreault, L.-É., Bechmann, A., Tarvainen, L., Klemedtsson, L., Shendryk, I., Dellwik, E., 2015. A LiDAR method of canopy structure retrieval for wind modeling of heterogeneous forests. *Agricultural and forest meteorology*, 201, 86–97.

Clark, M. P., Fan, Y., Lawrence, D. M., Adam, J. C., Bolster, D., Gochis, D. J., Hooper, R. P., Kumar, M., Leung, L. R., Mackay, D. S. et al., 2015. Improving the representation of hydrologic processes in Earth System Models. *Water Resources Research*, 51(8), 5929–5956.

de Koning, K., Broekhuijsen, J., Kühn, I., Ovaskainen, O., Taubert, F., Endresen, D., Schigel, D., Grimm, V., 2023. Digital twins: dynamic model-data fusion for ecology. *Trends in ecology & evolution*, 38(10), 916–926.

Dorman, J., Sellers, P. J., 1989. A global climatology of albedo, roughness length and stomatal resistance for atmospheric general circulation models as represented by the simple biosphere model (SiB). *Journal of Applied Meteorology and Climatology*, 28(9), 833–855.

Enevoldsen, P., 2017. Managing the risks of wind farms in forested areas: Design principles for Northern Europe.

Faivre, R., Colin, J., Menenti, M., 2017. Evaluation of methods for aerodynamic roughness length retrieval from very high-resolution imaging lidar observations over the Heihe Basin in China. *Remote Sensing*, 9(1), 63.

Finnigan, J., 2000. Turbulence in plant canopies. *Annual review of fluid mechanics*, 32(1), 519–571.

Floors, R., Badger, M., Troen, I., Grogan, K., Permien, F.-H., 2021. Satellite-based estimation of roughness lengths and displacement heights for wind resource modelling. *Wind Energy Science*, 6(6), 1379–1400.

Floors, R., Enevoldsen, P., Davis, N., Arnqvist, J., Dellwik, E., 2018. From lidar scans to roughness maps for wind resource modelling in forested areas. *Wind Energy Science*, 3(1), 353–370.

Kelly, M., Jørgensen, H. E., 2017. Statistical characterization of roughness uncertainty and impact on wind resource estimation. *Wind Energy Science*, 2(1), 189–209.

Kljun, N., Calanca, P., Rotach, M., Schmid, H. P., 2015. A simple two-dimensional parameterisation for Flux Footprint Prediction (FFP). *Geoscientific Model Development*, 8(11), 3695–3713.

Manabe, S., 1969. Climate and the ocean circulation: I. The atmospheric circulation and the hydrology of the earth’s surface. *Monthly weather review*, 97(11), 739–774.

Manabe, S., Smagorinsky, J., Strickler, R. F., 1965. Simulated climatology of a general circulation model with a hydrologic cycle. *Monthly Weather Review*, 93(12), 769–798.

Manders, A. M. M., Builtjes, P. J. H., Curier, L., Denier van der Gon, H. A. C., Hendriks, C., Jonkers, S., Kranenburg, R., Kuenen, J. J. P., Segers, A. J., Timmermans, R. M. A., Visschedijk, A. J. H., Wichink Kruit, R. J., van Pul, W. A. J., Sauter, F. J., van der Swaluw, E., Swart, D. P. J., Douros, J., Eskes, H., van Meijgaard, E., van Ulft, B., van Velthoven, P., Banzhaf, S., Mues, A. C., Stern, R., Fu, G., Lu, S., Heemink, A., van Velzen, N., Schaap, M., 2017. Curriculum vitae of the LOTOS–EUROS (v2.0) chemistry transport model. *Geoscientific Model Development*, 10(11), 4145–4173. https://gmd.copernicus.org/articles/10/4145/2017/.

Menenti, M., Ritchie, J. C., 1994. Estimation of effective aerodynamic roughness of Walnut Gulch watershed with laser altimeter measurements. *Water Resources Research*, 30(5), 1329–1337.

Monin, A., Obukhov, A., 1954. Osnovnye zakonomernosti turbulentnogo peremeshivanija v prizemnom sloe atmosfery (Basic laws of turbulent mixing in the atmosphere near the ground). *Trudy geofiz. inst. AN SSSR*, 24(151), 163–187.

Paulson, C. A., 1970. The mathematical representation of wind speed and temperature profiles in the unstable atmospheric surface layer. *Journal of Applied Meteorology (1962-1982)*, 857–861.

Pitman, A., 2003. The evolution of, and revolution in, land surface schemes designed for climate models. *International Journal of Climatology: A Journal of the Royal Meteorological Society*, 23(5), 479–510.

Queck, R., Bienert, A., Maas, H.-G., Harmansa, S., Goldberg, V., Bernhofer, C., 2012. Wind fields in heterogeneous conifer canopies: parameterisation of momentum absorption using high-resolution 3D vegetation scans. *European Journal of Forest Research*, 131(1), 165–176.

Raupach, M., 1992. Drag and drag partition on rough surfaces. *Boundary-Layer Meteorology*, 60(4), 375–395.

Raupach, M. R., 1994. Simplified expressions for vegetation roughness length and zero-plane displacement as functions of canopy height and area index. *Boundary-layer meteorology*, 71(1), 211–216.

Roussel, J.-R., Auty, D., Coops, N. C., Tompalski, P., Goodbody, T. R., Meador, A. S., Bourdon, J.-F., De Boissieu, F., Achim, A., 2020. lidR: An R package for analysis of Airborne Laser Scanning (ALS) data. *Remote sensing of environment*, 251, 112061.

Seginer, I., 1974. Aerodynamic roughness of vegetated surfaces. *Boundary-Layer Meteorology*, 5(4), 383–393.

Sellers, P. J., Dickinson, R., Randall, D., Betts, A. K., Hall, F. G., Berry, J. A., Collatz, G., Denning, A., Mooney, H. A., Nobre, C. A. et al., 1997. Modeling the exchanges of energy, water, and carbon between continents and the atmosphere. *Science*, 275(5299), 502–509.

Shaw, R. H., Pereira, A., 1982. Aerodynamic roughness of a plant canopy: a numerical experiment. *Agricultural Meteorology*, 26(1), 51–65.

Sogachev, A., Menzhulin, G. V., Heimann, M., Lloyd, J., 2002. A simple three-dimensional canopy–planetary boundary layer simulation model for scalar concentrations and fluxes. *Tellus B: Chemical and Physical Meteorology*, 54(5), 784–819.

Steffen, W., Sanderson, A., Tyson, P., Jäger, J., Matson, P., Moore, B., Oldfield, F., Richardson, K., Schellnhuber, H. J., Turner, B. et al., 2005. *Planetary Machinery: The Dynamics of the Earth System Prior to Significant Human Influence*. Springer Berlin Heidelberg, Berlin, Heidelberg, 11–80.

Stull, R. B., 2012. *An introduction to boundary layer meteorology*. 13, Springer Science & Business Media.

Taylor, P. A., Mason, P. J., Bradley, E., 1987. Boundary-layer flow over low hills. *Boundary-layer meteorology*, 39(1), 107–132.

Thom, A., 1971. Momentum absorption by vegetation. *Quarterly Journal of the Royal Meteorological Society*, 97(414), 414–428.

Tian, X., Li, Z., Van der Tol, C., Su, Z., Li, X., He, Q., Bao, Y., Chen, E., Li, L., 2011. Estimating zero-plane displacement height and aerodynamic roughness length using synthesis of LiDAR and SPOT-5 data. *Remote Sensing of Environment*, 115(9), 2330–2341.

Van den Hurk, B., Best, M., Dirmeyer, P., Pitman, A., Polcher, J., Santanello, J., 2011. Acceleration of land surface model development over a decade of GLASS. *Bulletin of the American Meteorological Society*, 92(12), 1593–1600.

Van Der Graaf, S. C., Kranenburg, R., Segers, A. J., Schaap, M., Erisman, J. W., 2020. Satellite-derived leaf area index and roughness length information for surface–atmosphere exchange modelling: a case study for reactive nitrogen deposition in north-western Europe using LOTOS-EUROS v2. 0. *Geoscientific Model Development*, 13(5), 2451–2474.

Van der Molen, M., Barten, S., Kruijt, B., Lootens, R., Snellen, H., Zhao, H., 2025a. ETC L2 fluxes from Loobos, 2022-12-31–2024-12-31.

Van der Molen, M., Barten, S., Kruijt, B., Lootens, R., Snellen, H., Zhao, H., 2025b. Etc l2 meteosens from Loobos, 2022-12-31–2024-12-31.

Van Ulden, A. P., Holtslag, A. A., 1985. Estimation of atmospheric boundary layer parameters for diffusion applications. *Journal of Applied Meteorology and Climatology*, 24(11), 1196–1207.

Weligepolage, K., Gieske, A., Su, Z., 2012. Surface roughness analysis of a conifer forest canopy with airborne and terrestrial laser scanning techniques. *International journal of applied earth observation and geoinformation*, 14(1), 192–203.

Wieringa, J., 1986. Roughness-dependent geographical interpolation of surface wind speed averages. *Quarterly Journal of the Royal Meteorological Society*, 112(473), 867–889.